

Electronic Supplementary Information

Heteroatom-doped carbon networks enabling robust and flexible silicon anodes for high energy Li-ion batteries

Rong Shao,^{a,b} Feng Zhu,^{a,b} Zhenjiang Cao,^a Zhengping Zhang,^{a,b} Meiling Dou,^{a,b} Jin

Niu,^{a,b,*} Baoning Zhu,^{c,*} Feng Wang^{a,b,*}

^a State Key Laboratory of Chemical Resource Engineering, Laboratory of Electrochemical Process and Technology for Materials, Beijing University of Chemical Technology, Beijing, 100029, P. R. China

^b Beijing Advanced Innovation Center for Soft Matter Science and Engineering, Beijing University of Chemical Technology, Beijing, 100029, P. R. China

^c Beijing Engineering Center for Environmental Pollution Control and Resource Utilization, College of Chemical Engineering, Beijing University of Chemical Technology, Beijing, 100029, P. R. China

* Corresponding Authors.

E-mail: niujin@mail.buct.edu.cn (J. Niu); bnzhu@mail.buct.edu.cn (B. Zhu); wangf@mail.buct.edu.cn (F. Wang); Fax: +86-10-64451996

1. Calculation details

(1) The theoretical capacity (C_T) of Si@CTSC anode was calculated as follows:

$$C_T = C_{Si} \times \omega_{Si} + C_C \times \omega_C = 4200 \text{ mAh g}^{-1} \times 84 \% + 372 \text{ mAh g}^{-1}$$

where C_{Si} is the theoretical capacity of Si (mAh g⁻¹), ω_{Si} is the mass fraction of Si in Si@CTSC anode, C_C is the theoretical capacity of C (mAh g⁻¹) and ω_C is the mass fraction of C in Si@CTSC anode (%).

(2) The gravimetric capacity (C_g) was measured to be 2547 mAh g⁻¹ at 0.2 A g⁻¹. The areal capacity (C_a) were calculated as follows:

$$C_a = C_g \times m_a = 2547 \text{ mAh g}^{-1} \times 1 \text{ mg cm}^{-2} = 2.55 \text{ mAh cm}^{-2}$$

(3) The values of b parameter was calculated as follows:⁴⁷

$$i = k_1 v + k_2 v^{1/2} = av^b$$

where v is the scan rate; k_1 , k_2 , and a are constants.

(4) The binding energy (BE) was calculated using the equation:⁴³

$$BE = E_T - E_C - E_{Si/Cu}$$

where E_T is the total energy of the Si/C system, E_C is the energy of the undoped or N, O-doped carbon system, and $E_{Si/Cu}$ is the energy of the free Si/Cu atom. A more negative value of BE means a stronger binding interaction between Si and the carbon matrix.

(5) The energy density (E , Wh kg⁻¹) of the full cell can be calculated as:⁴⁹

$$E = C \times V/W$$

where C is total capacity (Ah), V is working voltage (V), W is total weight of the

electrode materials (kg).

The theoretical energy density (E_T) of Si@CTSC//LCO was calculated as follows:

$$\begin{aligned} E_{T=C} \times V/W &= 3588 \text{ mAh } g^{-1} \times 12.5 \text{ mg} \times 3.6 \text{ V} / (12.5 + 250) \text{ mg} \\ &= 615 \text{ Wh } kg^{-1} \end{aligned}$$

2. Supplementary figures, tables and related discussion

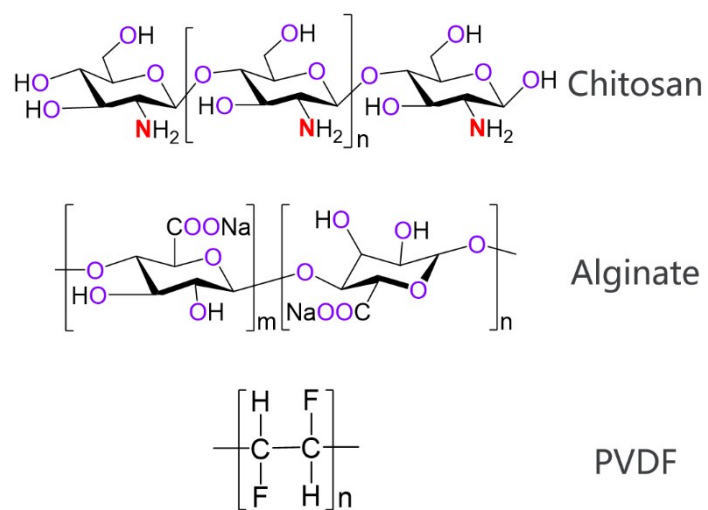


Fig. S1 Molecular structures of CTS, ALG, and PVDF.

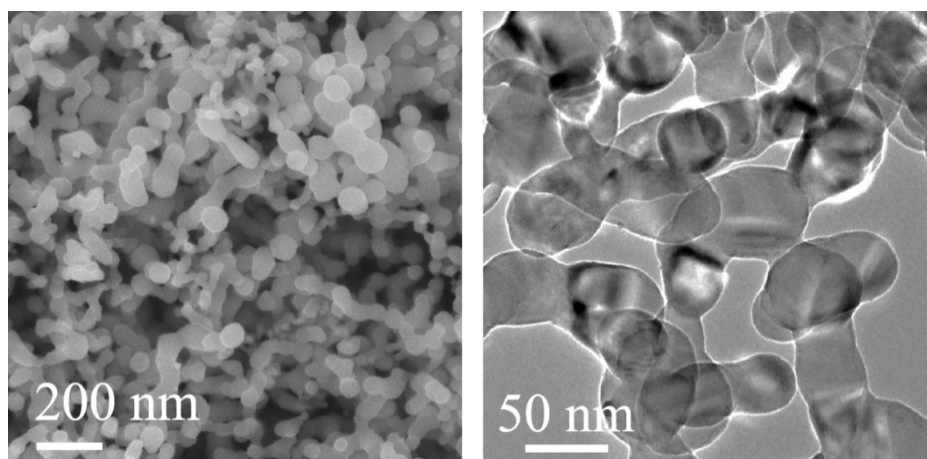


Fig. S2 (a) SEM and (b) TEM images of Si NPs.

The majority of Si NPs used in our work had spherical shape with diameter in a range of 30-50 nm.

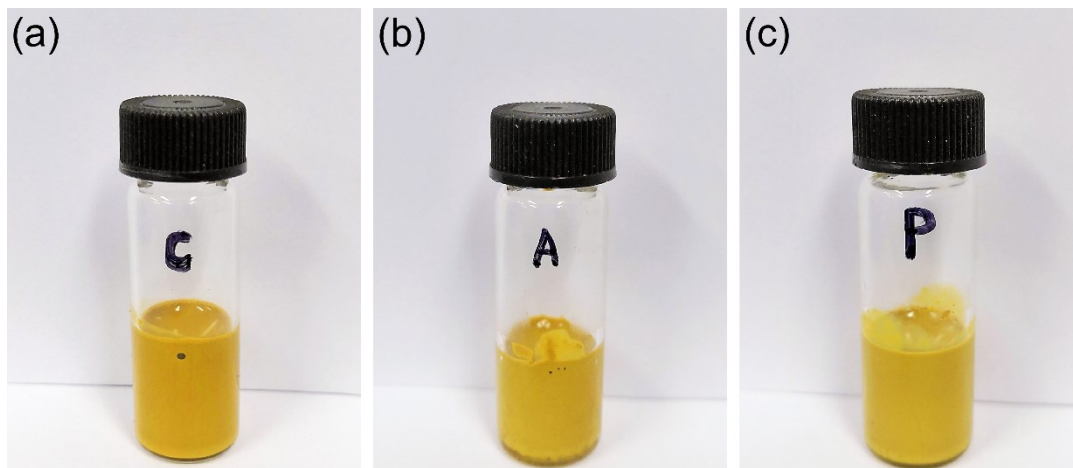


Fig. S3 Photographs of Si NPs dispersed in (a) CTS, (b) ALG, and (c)PVDF solutions after standing for 24 h.

As shown in Fig. S3, Si NPs could be well dispersed in these three polymer solutions (CTS in water, ALG in water, and PVDF in NMP) without any precipitation even after standing for 24 h.

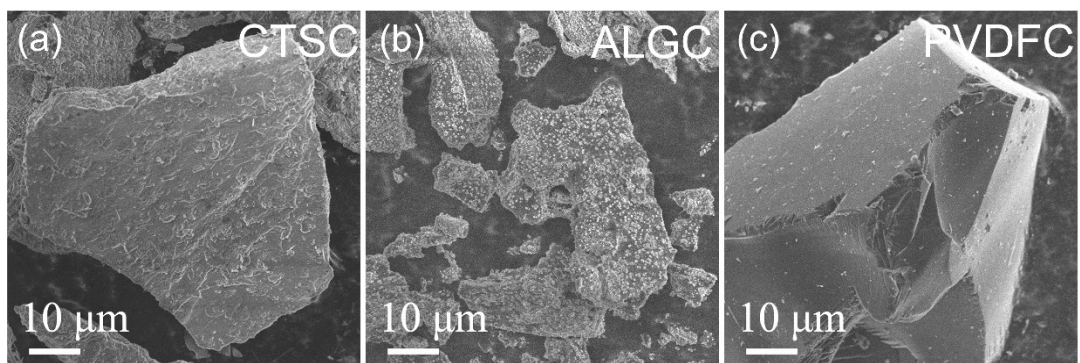


Fig. S4 SEM images of (a) CTSC, (b) ALGC, (c) PVDFC.

These three binders, when carbonized individually, had a bulk-shaped morphology. However, when mixed with Si NPs, they could be evenly coated on the Si surface. This phenomenon further proved the superiority of this method.

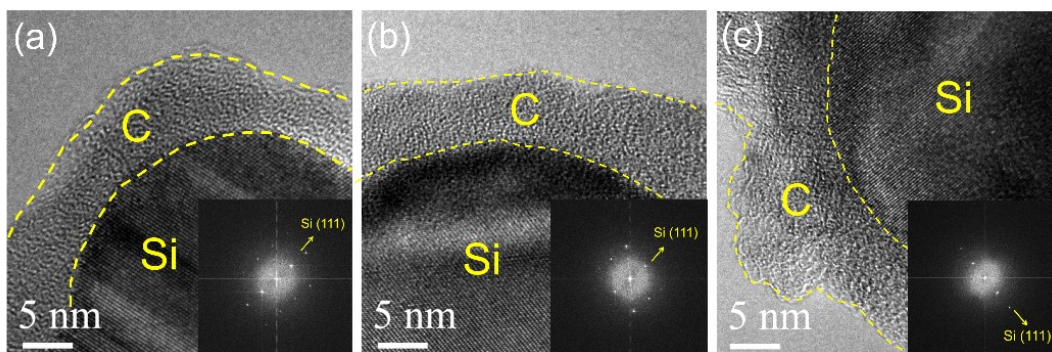


Fig. S5 High-magnification TEM image and FFT patterns of (a) Si@CTSC, (b) Si@ALGC, and (c) Si@PVDFC.

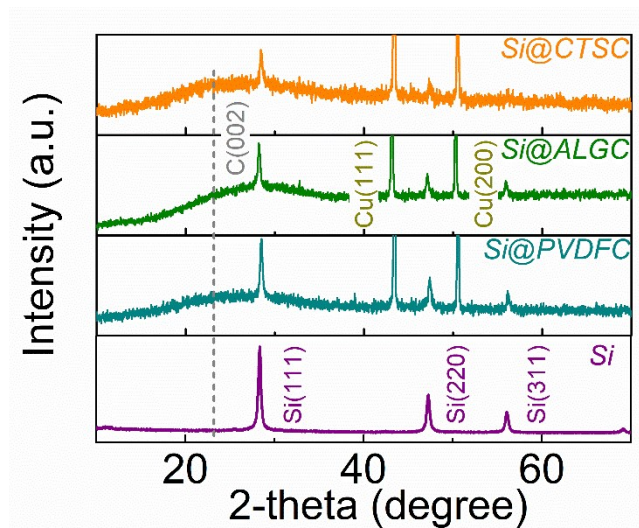


Fig. S6 XRD pattern of Si@CTSC, Si@ALGC, Si@PVDFC, and Si composites.

The peaks of all patterns showed sharp peaks at 28.4, 47.3, and 56.1°, which were ascribed to the (111), (220), and (311) lattice planes of Si, respectively (JCPDS card No. 27-1402). A broad and weak diffraction peak located in the 2θ range of 21-23° was associated with the (002) plane of amorphous carbon.

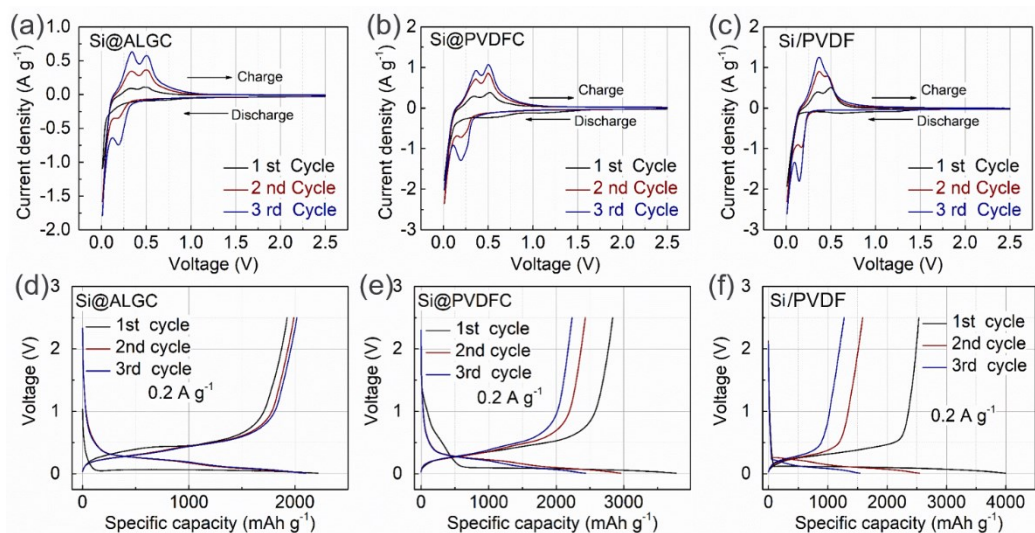


Fig. S7 CV curves at $0.1 mV s^{-1}$ and GCD profiles at $0.2 A g^{-1}$ of Si-based anodes. (a, d) Si@ALGC, (b, e) Si@PVDFC, and (c, f) Si/PVDF anodes.

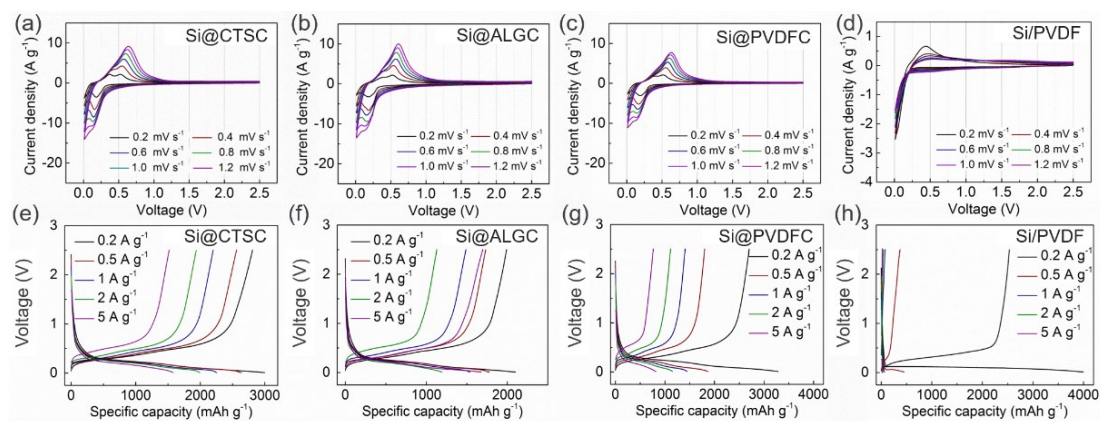


Fig. S8 CV curves at different scan rates ($0.2\text{--}1.2\text{ mV s}^{-1}$) and GCD profiles at different current densities ($0.2\text{--}5\text{ A g}^{-1}$) of Si-based anodes. (a, e) Si@CTSC, (b, f) Si@ALGC, (c, g) Si@PVDFC, and (d, h) Si/PVDF anodes.

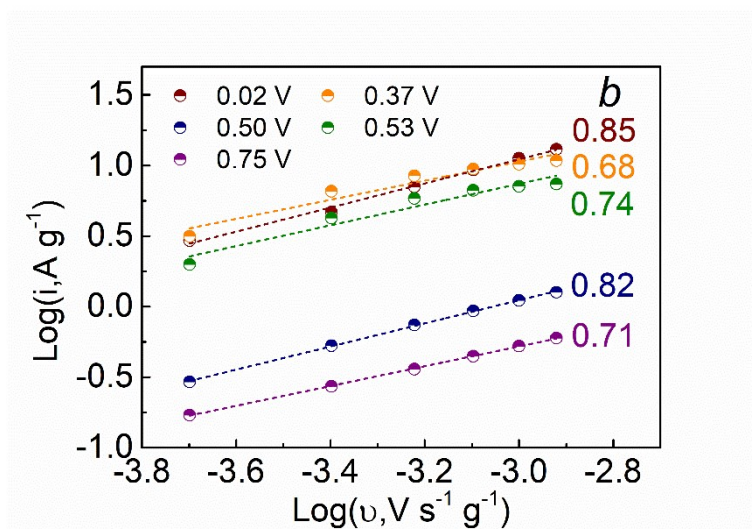


Fig. S9 b values of Si@CTSC anode at different voltages for anodic scan.

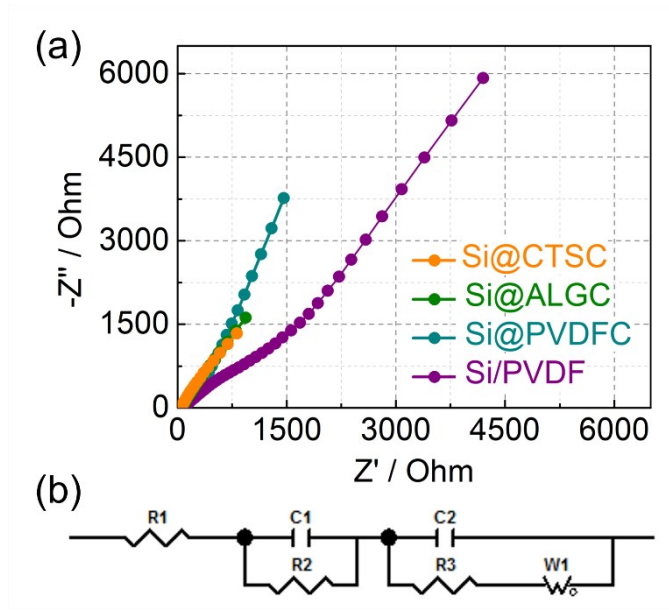


Fig. S10 (a) Nyquist plots of Si@CTSC, Si@ALGC, Si@PVDFC, and Si/PVDF anodes. (b) The simulation equivalent circuit.

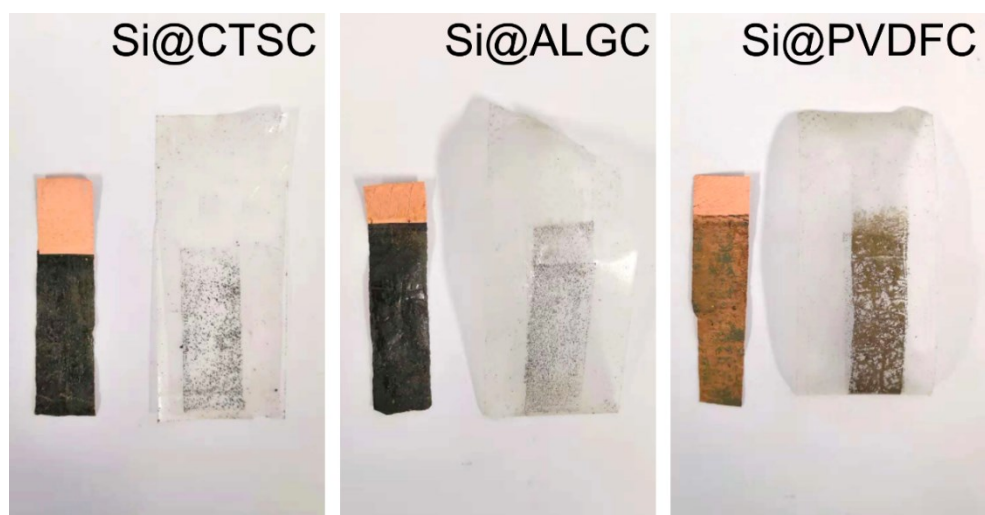


Fig. S11 Pictures of tapes and electrodes after the 180 ° peeling test.

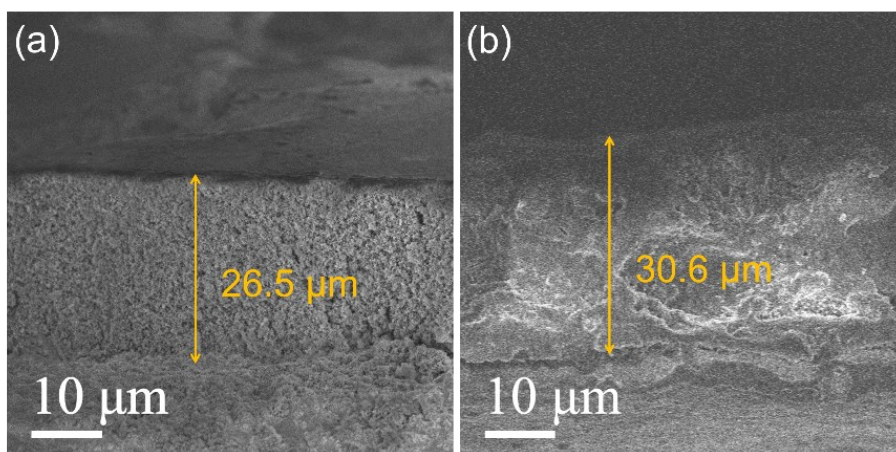


Fig. S12 Cross-sectional images of the (a) fresh and (b) cycled Si@CTSC anode (in delithiation state).

The volume expansion rate of Si@CTSC anode after cycling was about 115%, showing a small volume expansion without obvious cracks.

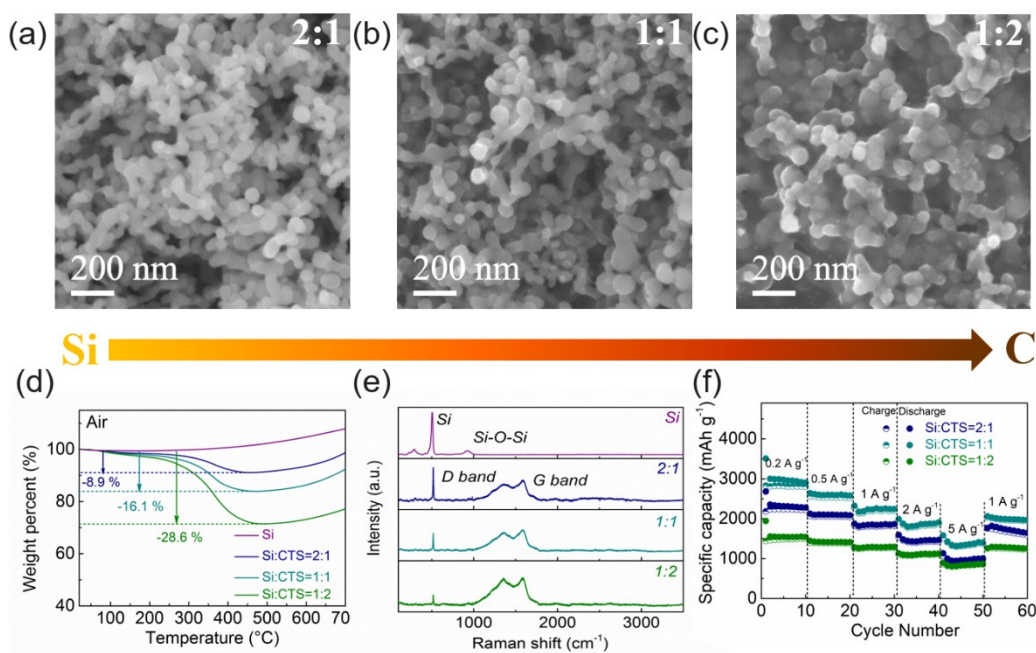


Fig. S13 SEM images of Si-based materials after pyrolysis at 450 °C with different precursor ratios (Si to CTS) (a) 2:1, (b) 1:1 (Si@CTSC), and (c) 1:2. (d) Thermogravimetric curves (e) Raman spectra. (f) Rate capabilities from 0.2 to 5 A g⁻¹.

To further explore the effects of pyrolysis temperature and precursor ratio (Si to CTS) on the formation of interfacial bonding as well as the electrochemical property, comparative Si/C anodes were also prepared (Fig. S13 and Fig. S14). SEM images showed that Si NPs were well coated by CTSC, the thickness of CTSC shell obviously increased as the carbon content increased. The TGA results shown in Fig. S10d revealed the weight content of carbon increased as the CTS content increased. The optimized pyrolysis temperature of 450 °C with a precursor ratio of 1:1 exhibited the best performance for Li-ion storage.

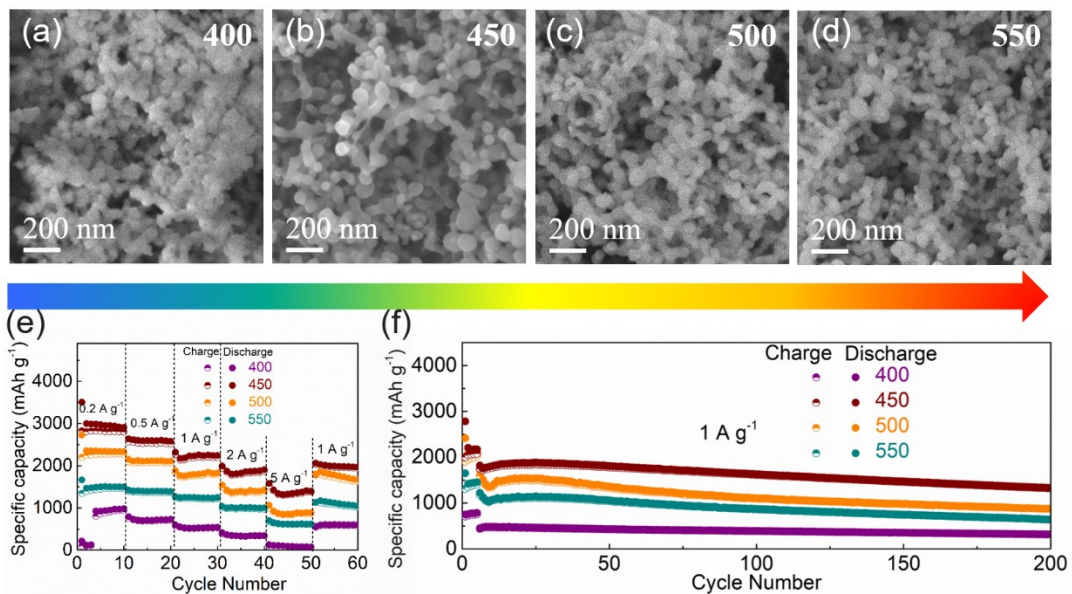


Fig. S14 SEM images of Si-based materials with the same precursor ratio of 1:1 after pyrolysis at (a) 400 °C, (b) 450 °C (Si@CTSC), (c) 500 °C and (d) 550 °C. Electrochemical performance of Si-based anodes. (e) Rate capabilities from 0.2 to 5 A g⁻¹. (f) Cycling performance at 1 A g⁻¹ (the initial 5 cycles were at 0.2 A g⁻¹).

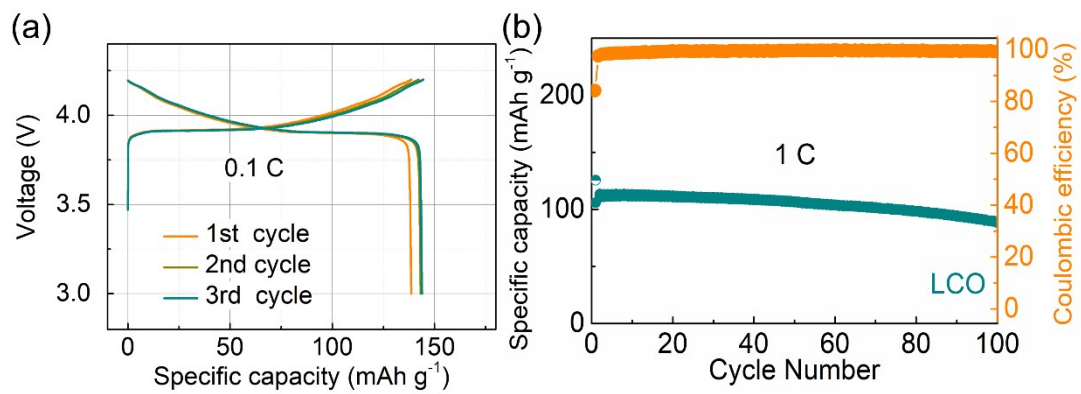


Fig. S15 Electrochemical performance of LCO cathode. (a) GCD profiles at 0.1C. (b) Cycling performance at 1C.

Table S1 Comparison of the electrochemical performance for Si-based anodes.

Sample	Si Content (%)	ICE (%)	Gravimetric capacity^a	Areal capacity^b	Ref.
Si@CTSC	84	81	3144 mAh g ⁻¹ at 0.2 A g ⁻¹	2.55 mAh cm ⁻²	This Work
Si@C@ZIF-67-800	51	79	978 mAh g ⁻¹ at 1 A g ⁻¹	-	29
HCC-M-Si	57.1	73	1584 mAh g ⁻¹ at 0.4 A g ⁻¹	0.5 mAh cm ⁻²	30
Si nanosheet	80	47.7	1327 mAh g ⁻¹ at 0.4 A g ⁻¹	2.48 mAh cm ⁻²	31
Si-PBI	61.5	60.3	1336 mAh g ⁻¹ at 1 A g ⁻¹	-	32
PEDOT:PSS/SiNP	80	78	2400 mAh g ⁻¹ at 0.5 A g ⁻¹	2.4 mAh cm ⁻²	33
Silicene flowers	80	74	2051 mAh g ⁻¹ at 0.4 A g ⁻¹	1.84 mAh cm ⁻²	34
Si@CNT/C	84.5	83	2704 mAh g ⁻¹ at 0.2 A g ⁻¹	5.58 mAh cm ⁻²	35
GDY-Si ₂	80.4	75	1855 mAh g ⁻¹ at 0.2 A g ⁻¹	1.06 mAh cm ⁻²	36

^{a)}Gravimetric capacity and ^{b)} Areal capacity are all based on total material mass on anode.

Table S2 The simulation results of EIS for Si-based anodes.

Sample	ESR (R_1, Ω)	R_f (R_2, Ω)	R_{ct} (R_3, Ω)
Si@CTSC	3.3	3.2	7.1
Si@ALGC	3.6	4.3	11.3
Si@PVDFC	3.6	4.6	18.6
Si/PVDF	3.8	10.2	37.1

Table S3 Comparison of the electrochemical performances for LIBs.

Sample	Battery Type	Mass loading	Voltage (V)	Average Voltage (V)	ICE (%)	Cycling Performance	Capacity (mAh)	Energy Density (Wh kg ⁻¹)	Ref.
Si@CTSC//LCO	Pouch	260 mg	3-4.2	3.75	94.7	101.8 mA h g ⁻¹ after 100 cycles at 0.42 A g ⁻¹	30.4	540	This Work
Si@CTSC//LCO	Coin	17 mg	3-4.2	3.67	92.0	105.6 mA h g ⁻¹ after 100 cycles at 0.42 A g ⁻¹	2.61	561	This Work
HCC-M-Si//LiCoO ₂ /LiNi _{0.5} Mn _{1.5} O ₄	Coin	31 mg	3-4.2	3.7	62	44.2 mAh g ⁻¹ after 100 cycles at 0.4 A g ⁻¹	1.38	486	30
Si/C//LCO	Coin	20 mg	2.5–4.35	3.75	96	111.3 mAh g ⁻¹ after 50 cycles at 0.07 A g ⁻¹	2.29	416	31
Silicon-PBY//LCO	Coin	-	2.5-4.0	3.5	90.3	55 mAh g ⁻¹ after 100 cycles at 0.13 A g ⁻¹	-	367	32
SN-MCB//NCA80	Coin	16 mg	2.5–4.1	3.6	94	152 mAh g ⁻¹ after 300 cycles at 0.2 A g ⁻¹	2.52	340	44
YS-Si/C//LFP	Coin	-	2-4	2.9	90.9	134 mAh g ⁻¹ after 300 cycles at 0.05 A g ⁻¹	-	435	45
EB-1//LCO	Coin	20 mg	3–4.2	3.54	89.3	1.45 mA h cm ⁻² (~61 mAh g ⁻¹) after 100 cycles at 0.03 A g ⁻¹	2.49	371	46

N-PSi@C//LCO	Coin	20 mg	^{3-4.3}	3.67	88.8	127 mAh g ⁻¹ after 300 cycles at 0.2 A g ⁻¹	2.7	536	47
--------------	------	-------	------------------	------	------	---	-----	-----	----
